Geomorphology 393 (2021) 107913

Contents lists available at ScienceDirect

Geomorphology

journal homepage: www.elsevier.com/locate/geomorph

Modelling early medieval flood-induced breaching of a coversand ridge in the IJssel valley, Rhine delta, the Netherlands

J.R. Dierx [a], A. Bomers [a,*], B. van der Meulen [b], K.M. Cohen [b], S.J.M.H. Hulscher [a]

[a] Dept. Water Engineering & Management, University of Twente, Enschede, The Netherlands
[b] Dept. Physical Geography, Utrecht University, Utrecht, The Netherlands

ARTICLE INFO

Article history:
Received 1 June 2021
Received in revised form 13 August 2021
Accepted 13 August 2021
Available online 19 August 2021

Keywords:
Breach erosion
Flood modelling
Palaeoflood model
River avulsion
Avulsion by annexation
Rhine delta

ABSTRACT

Connecting geologically mapped data to numerical modelling can help in understanding river landscape evolution. This study focuses on flood-induced breaching of the coversand ridge in the IJssel valley floodplain (Rhine delta, the Netherlands). The development of the breach would explain why this river branch came into existence in early medieval times. Prior to the breaching, the coversand ridge formed a barrier for the Rhine River to discharge towards the north. A palaeoflood model was coupled to a local sediment transport model to predict sediment transport rates in two competing coversand ridge breaches. The results show that the breach at the current IJssel River location was expected to expand earlier and faster in time for various upstream discharge waves and initial breach dimensions. This provides quantitative argumentation for the IJssel river avulsion case to have been triggered by the breaching of the coversand ridge during a large palaeoflood.

1. Introduction

Combining qualitative and quantitative insights in past fluvial processes is key in understanding river landscape evolution and modern-day river functioning in normal and flooded conditions. Mapping evidence together with hydrodynamic modelling has proven to be valuable in morphodynamic studies on channel erosion, bank stability and discharge partitioning over decadal to centennial time scales. These studies contribute to insights in historic cases and modern river management issues (e.g., Kleinhans et al., 2010; Hajek and Wolinsky, 2012). Furthermore, combining hydrodynamic modelling with mapping evidence is of use for major flood studies that have the goal of upgrading geomorphic and historic information to quantified estimates of flood magnitudes and durations. These quantified magnitudes of palaeofloods can be used in return time statistics to improve the assessment of recurrence of discharge extremes in the twenty-first century (e.g., Benito and Thorndycraft, 2005; Bomers et al., 2019b).

Geomorphological mapping and dating of component landforms is a first step in understanding landscape evolution, resulting in both qualitative and quantitative inferences regarding the functioning of the river-floodplain system in the past. Examples of such studies are Stouthamer and Berendsen (2000), Burge (2006) and Macklin et al. (2015), revealing the typical kinematics of past fluvial processes. However, such studies typically cannot provide information about the exact duration and supposed dynamics of these fluvial processes (Kleinhans et al., 2013). Providing such insight requires numerical models to be set up for palaeo-cases, whether for the in-channel part of river systems, their floodplains, or both. Rare examples of such approaches come from the Lower Rhine system in the Netherlands, notably Kleinhans et al. (2010) and Kleinhans et al. (2008, 2011) who assessed a semi-cyclic discharge and sediment partitioning at the upper most bifurcation of the Rhine delta, but these applications targeted normal river flow and bedload transport and hereto focused on modelling in-channel hydraulics.

Numerical modelling studies can also be conducted for situations where river channels initiate through inundated floodplains. Such studies allow detailed reconstructions of avulsion development (e.g., Smith et al., 1989). So far, numerical modelling studies in avulsion contexts have focused on floodwater leaving the main channel by entering levee-breaching crevasse channels (e.g., Slingerland and Smith, 1998) and on maturation of crevasse splays (e.g., Millard et al., 2017). These studies have recognized the case-by-case dependencies of avulsions, highlighting that only some succeed, because of other sets of processes (Hajek and Edmonds, 2014: incisional vs. progradational avulsions). The evolution of river diversion is a time-dependent morphodynamic process. Therefore, detailed specifications of initial and boundary conditions are required for a quantitative analysis. This has meant that numerical model studies so far have mainly been inspired on the 1870s Saskatchewan avulsion into Cumberland Lake in central Canada (an inland basin to which the rivers avulsed repeatedly during the Holocene; e.g., Morozova and Smith, 2000), and the deltaic avulsion

* Corresponding author.
E-mail address: a.bomers@utwente.nl (A. Bomers).

https://doi.org/10.1016/j.geomorph.2021.107913

belt development in the Atchafalaya plains in the Lower Mississippi in the USA (also into an area used by the parent river in earlier times; e.g., Törnqvist et al., 1996).

In this study, we develop a numerical model for the triggering of an 'avulsion by annexation', where floodwaters invade an area not part of the floodplain before because erodible landforms bounding the original floodplain were overtopped and breached. The river system hosting this case and producing the breach initiating flood is that of the Lower Rhine in Germany and the Netherlands (Fig. 1). The Lower Rhine is the alluvial reach that begins where the river leaves the bedrock-confined Middle Rhine and that grades from valley to delta in the Dutch-German border area (Erkens et al., 2011). The delta is traversed by three deltaic branches, the Waal, Nederrijn and IJssel rivers, of which the first two flow westward and have been known since Roman times (first centuries CE) and the latter one flows northward and is of Early Medieval origin (Makaske et al., 2008). The onset age for the IJssel avulsion is put at some point between 600 and 800 CE (Makaske et al., 2008; Cohen et al., 2012), a time frame for which paleohydrological modelling of Rhine flooding at full Lower Rhine scale has recently become available (Van der Meulen et al., 2021).

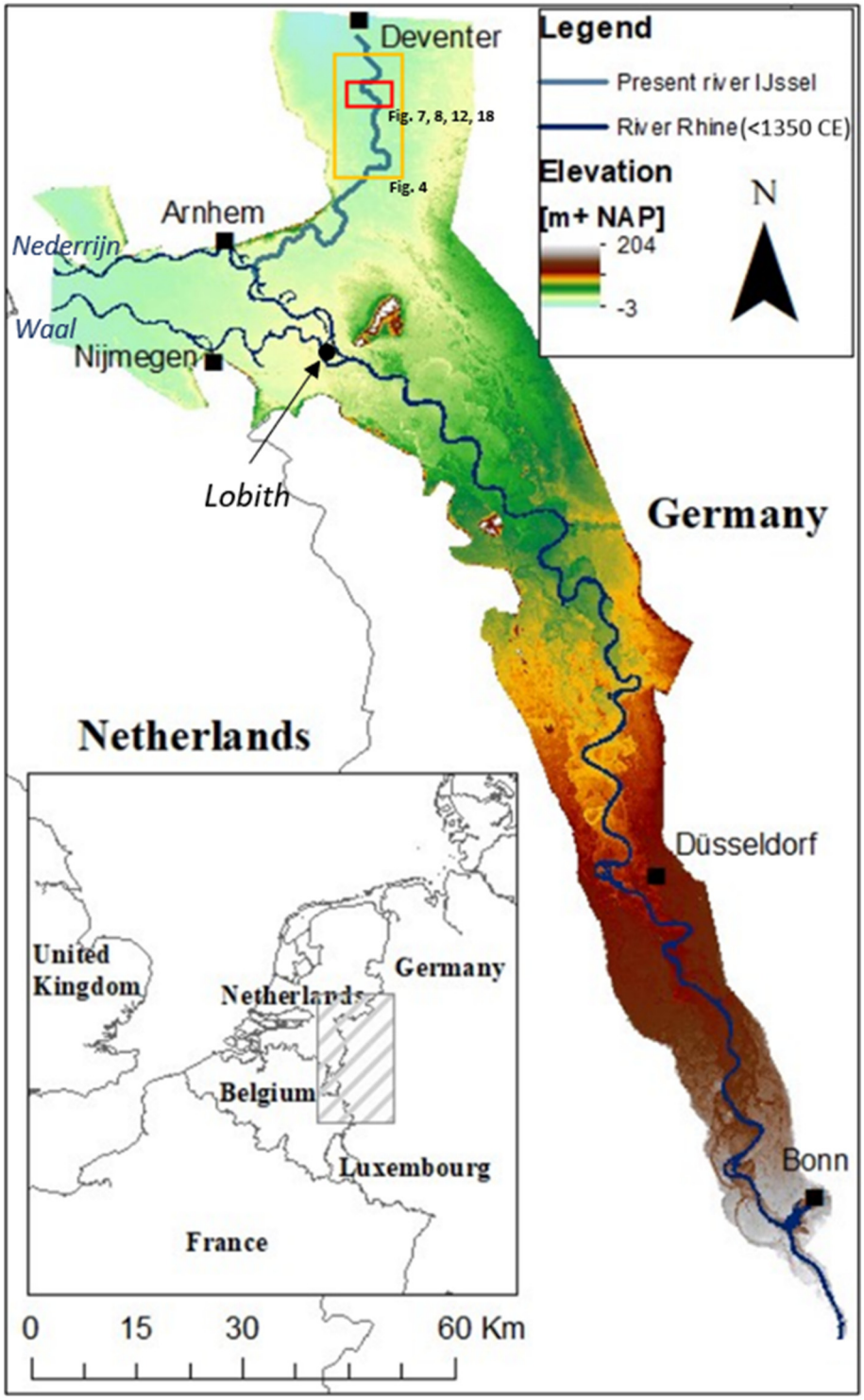

Fig. 1. DEM of the full palaeoflood model domain with the early medieval Rhine River course from Van der Meulen et al. (2020).

From LiDAR-aided shallow geological mapping (Cohen et al., 2009, 2012) it is evident that the IJssel branch dissects a former floodplain bordering divide comprised by coversand ridges and further periglacial alluvial erodible substrate, landforms essentially inherited from Lateglacial times. Triggering of the IJssel avulsion would have involved the breaching of this drainage divide. Mapping has identified breach features in the divide morphology to have partially preserved at some distance of the eventual meandering river. Closer to the river, a multi-channel crevasse splay complex from when the avulsion was young preserved dissecting the divide, but surviving breach channel morphology attributable to the triggering stage is not evident.

To explain these combined findings, in regional literature a qualitative hypothesis exists for the course of events at the very begin of the avulsion (Cohen and Lodder, 2007; Cohen et al., 2009), beginning with the establishment of two breach channels during some early medieval major flood event, which each then started to enlarge as the flood event proceeded. The simultaneous breaches are reckoned to have been in competition in drawing discharge, leading one to fail as a river and preserve in isolation, while the other one succeeded and became the established avulsion path (and eventually, the IJssel River). This study evaluates this hypothesis quantitatively, by modelling the flooding and channel carving conditions at the critical breach locations. The approach can help to provide a minimum flood magnitude needed to trigger the double breaching, as well as assessment of the pacing of the competitive development of the breaches, and insight into how and why the avulsion path was favoured. In highlighting competitive development in multi-channel initial avulsions states, parallels may be drawn with competition occurring between crevasse channels sustaining avulsion splay complexes (Smith et al., 1989; Hajek and Edmonds, 2014), with the caveats that (i) the localized initiation of divide breach channels differs from that of levee-cutting crevasses, and that (ii) this study focuses on short-lived breach channels from the triggering stage of an avulsion, while avulsion belt crevasse channels are inferred to represent a subsequent stage of much longer duration (Makaske et al., 2008; Cohen et al., 2009, 2012).

We set up a coupled hydrodynamic-sediment transport model for assessing the effects of historic floods (modelled for the German-Dutch Lower Rhine, including a reconstructed divide area) on potential flood-induced breach development (modelled for the breach channels in the divide region). The outline of the paper is as follows. In Section 2, information about the formation of the IJssel River is given. In Section 3, the state-of-the-art coupled hydrodynamic-sediment transport model is described, which is used to identify if the historic flood events were powerful enough to develop a breach. Section 4 describes the findings of the model simulations. The paper ends with a discussion focused on the terrain reconstruction, the hydraulic model parameterisation and the sediment transport model (Section 5) and conclusions (Section 6).

2. Geographical Setting: the IJssel River avulsion

The Lower Rhine River in its German valley and Dutch delta parts (Fig. 1), has been freely meandering up to historic times. Since Late Medieval times, dikes have been raised along the major branches and in younger centuries also the channel itself became increasingly human-modified. In the nineteenth century, many interventions were carried out that confined channel flow and halted lateral migration (Kalweit et al., 1993). Close to the German-Dutch border (Lobith in Fig. 1), the Rhine River first bifurcates into the two river branches Waal and Nederrijn (Fig. 2). Currently, the river Waal represents the largest Rhine River branch with an engineering controlled discharge partitioning between the branches Waal (67%) and Nederrijn (33%), whereas in medieval times the partitioning oscillated with the Nederrijn for many centuries drawing the majority (Kleinhans et al., 2011). A second bifurcation exists near Arnhem (Fig. 1), which splits discharge between the continuing Nederrijn (67%) and the IJssel River (33%) that exists since early medieval times and of which the initiation is the topic of this study.

The avulsion that created the IJssel River, at some moment in the first millennium CE (beginning in sixth or seventh century CE, see below) is an extreme case of avulsion by annexation. Establishment of the branch enlarged the Rhine delta with substantial area (~400 km^2 on a total of 2000 km^2; e.g., Erkens, 2009). More importantly, it changed the partitioning of channel and floodwater discharge via Nederrijn and Waal towards the west (debouching into the North sea) and the northward IJssel (debouching into the central Netherlands lagoon and Wadden Sea; Fig. 1). Routing of discharge to the former area was reduced by up to ~25% in late medieveal times (thirteenth to fifteenth century CE) when the IJssel branch was most active and grew largest (Ente, 1971; Hesselink, 2002; van Popta et al., 2020), a time when economic activity also boomed along this branch (Hanseatic trade league). In later centuries, the IJssel branch lost discharge in favour to the westward branches (developments summarized in Kleinhans et al. (2011)). In the nineteenth century, human interventions in the floodplain and the river channel bifurcations had made the Rhine channel network a managed one, and the controlled partitioning of IJssel discharge has been set to 9–15% in the modern situation (Spruyt and Asselman, 2017).

Cohen and Lodder (2007) first hypothesised that the triggering of the IJssel avulsion could be the result of an extreme flooding event,

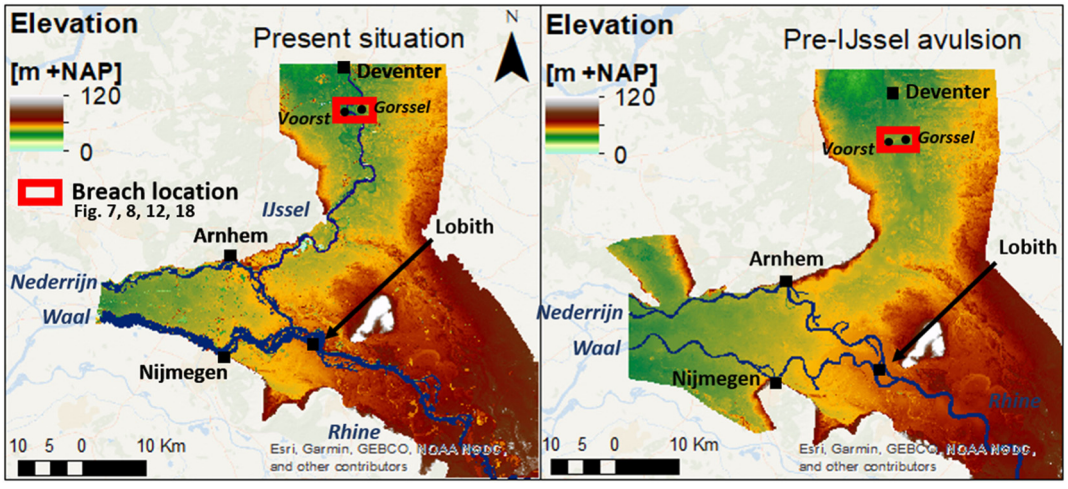

Fig. 2. Present vs. Pre-embanked situation of the northern part of the study area. A close-up of the breach location is provided in Fig. 7.

and that geomorphologically mapping and inferring past flood heights in combination with numerical modelling could be a way to assess the magnitude of that flood event. The area critical to consider in the triggering of the avulsion is the very northeast of the Rhine delta plain (Fig. 2). LiDAR and borehole mapping activities in that reach of the modern IJssel River (Cohen et al., 2009) identified: (i) the width and structure of the matured IJssel meander belt, (ii) the width and structure of an adjacent crevasse complex, reckoned a multi-channel youngest stage of IJssel activity (an avulsion belt, cf. Stouthamer and Berendsen, 2001), (iii) the presence of relatively isolated breach channel-splay complexes along the outer rim of the crevasse complex, where IJssel floodwaters had cut through coversand ridges (landforms of Late Pleistocene age constituting the floodplain substrate), and (iv) a particular region in the IJssel valley (Voorst-Gorssel area) where breached coversand ridges were relatively highest (Figs. 2 and 3). In this region, the IJssel meander belt, crevasse complex and floodplain are relatively narrowest, and the meander belt longitudinal gradients locally steepest, supporting that this was a coversand ridge breaching reach.

In the last decade, several studies on flooding activity during the first millennium CE have revealed that episodes of increased flood activity occurred in the sixth to eighth century CE when the IJssel branch began to form (Makaske et al., 2008; Cohen et al., 2009; Groothedde, 2010). Local dendrological indications for this are reported in Sass-Klaassen and Hanraets (2006), speculating it was an IJssel-avulsion related signal. Jansma (2020) established that the dendrohydrological signal reproduces delta wide and that in the beginning of the 7th century particularly large inundation events occurred. Toonen et al. (2017) also identified the 6th–8th century as the most flood-intensive episode of the Lower Rhine record in the first millennium CE based on sedimentary signals in cores from series of oxbow lakes (Toonen, 2013; Cohen et al., 2016; Toonen et al., 2020). Furthermore, geomorphological and geoarchaeological analysis of heights of natural levees and their human occupancy confirm the early medieval flood episode (Pierik et al., 2017; Pierik and van Lanen, 2019).

Budget analysis of the quantities of overbank deposition (Harbers and Mulder, 1981; Erkens, 2009; Erkens et al., 2012) reveal apex-back-stepping of the Rhine-apex in the first millennium BCE (Stouthamer and Berendsen, 2000; Gouw and Erkens, 2007). This primed the delta apex region for the IJssel avulsion, explaining why rare large floods in early medieval times could breach the Voorst-Gorssel coversand ridge, whereas similar magnitude millennial floods in earlier parts of history did not (Cohen et al., 2009, 2012, 2016).

In the breached divide area, the IJssel River dissects a Pleistocene substrate topped with coversand deposits (Fig. 3). These landforms formed during the last part of the Pleistocene between 30,000 to 11,700 years ago because of aeolian sand transport, burying an infilled valley of the Rhine abandoned earlier in the last glacial period (Busschers et al., 2007). Because of differences in genesis (aeolian vs fluvial transport) and age (long exposed to soil formation vs. freshly deposited) the coversands and IJssel fluvial sands are easily distinguished when mapping. Furthermore, the coversand textural composition (decalcified, fine sands, moderately well sorted (e.g., Makaske et al. (2008); Cohen et al. (2009)) is fairly homogenous compared to riverine sands (carbonates bearing, heterolithic, intercalated silt and clay beds).

Detailed mapping (Cohen et al., 2009, 2012) revealed the preserved breach near Voorst to have a topographic depth of approximately 2 m from the crest of the coversand ridge and a width of approximately 70 m. Borehole interpretations showed that 2 m of sandy infill occupies this original breach channel (Fig. 3). Thus, it is estimated that the breach channel when functioning had a depth of ~4 m. The original widths and associated coversand ridge saddle elevation of the breach near Gorssel cannot be read from LiDAR data, as this breach has evolved into a meander belt. Therefore, its best guess elevation estimate is that projected from the breach near Voorst.

The development of the breach channels through the coversand ridge divide (Figs. 3 and 4) and the tying of these landforms to the high magnitude floods that would have triggered the IJssel avulsion, are the elements that this study investigates further through numeric modelling and quantitative analysis. In that modelling, the chain of events creating the breach channels and determining their faith is the following:

- Rising floodwaters gradually inundated the area from the south during large discharge events;
- Breaches were initiated at two locations (near Gorssel and Voorst (Fig. 2)) once floodwaters had risen higher and overtopped the coversand ridge;
- For some unknown duration (not resolvable with geological dating methods) the two breaches functioned in competition, but eventually

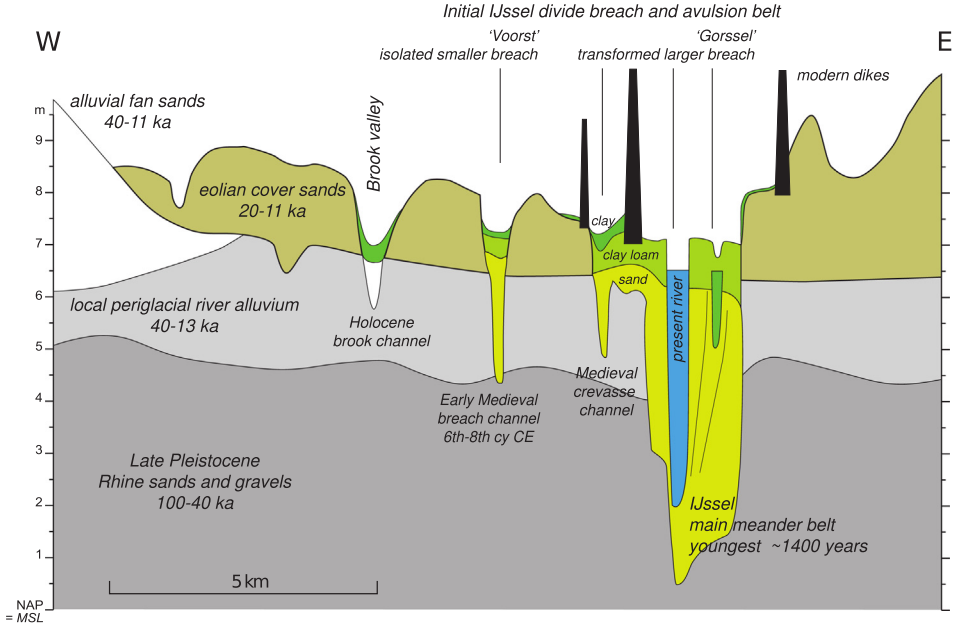

Fig. 3. Schematic section showing architecture of young IJssel river deposits dissecting sandy substrate of the breach area. After Cohen et al. (2009, modified). Location of this schematic section is given in Fig. 4.

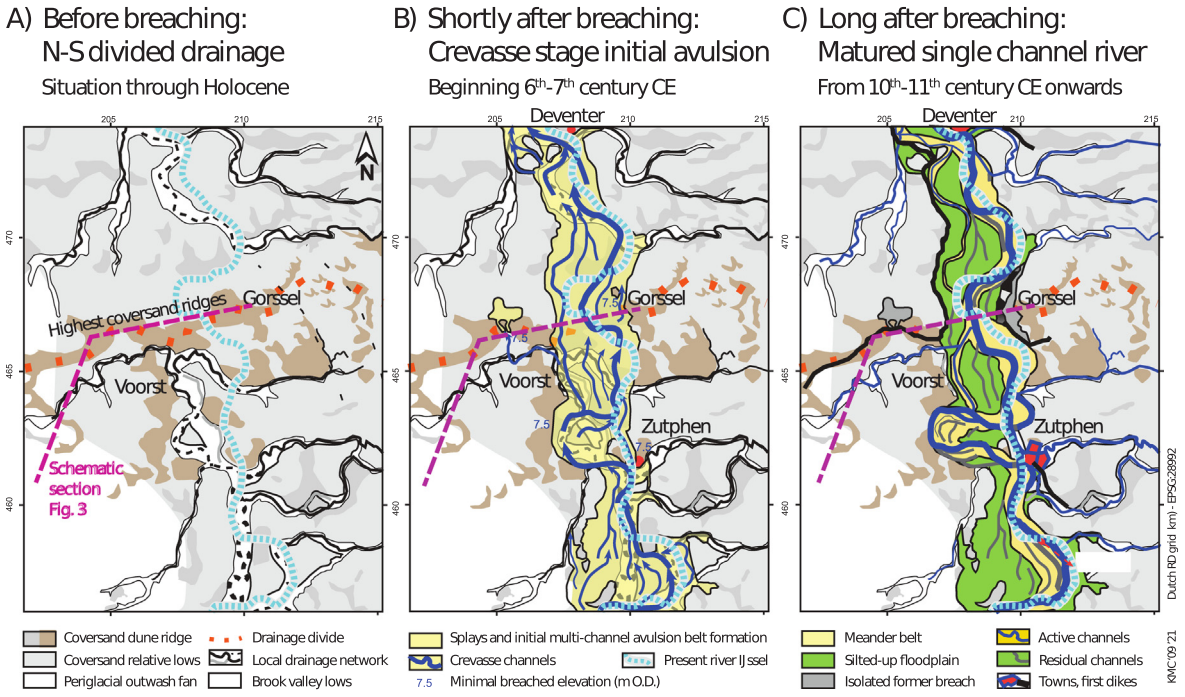

Fig. 4. Mapping reconstruction of the breach area in three stages before and after breaching (Cohen et al., 2009, modified). Location is given in Fig. 1.

(possibly during passage of a single major flood, possibly needing a repeat event) the Gorssel breach became the sole functioning one.

3. Modelling approach

In the modelling, the palaeo-DEM constructed by Van der Meulen et al. (2020) and the hydrodynamic model set-up of Van der Meulen et al. (2021) were used as starting points. Both materials represent the situation of the Rhine and IJssel floodplain around 800 CE, and in the IJssel divide area represents a situation where the coversand ridge had been breached, but a main channel for the IJssel River had not yet matured (e.g. that of Fig. 4B). For the purpose of this study, a divide topography before breaching was required, which was achieved by making local modifications to the palaeo-DEM in the divide area. Accordingly, minor local modification of the roughness classifications and model set-up were also carried out. First, the hydrodynamic model is described in Section 3.1. The results of this hydrodynamic model serve as input of a local sediment transport model to gain insight in the potential breach development. This sediment transport model is presented in Section 3.3. The proposed methodology is presented in Fig. 5.

3.1. Palaeoflood model of the Lower Rhine valley and delta

The hydrodynamic modelling in Van der Meulen et al. (2021) covers the entire floodplain of the Lower Rhine system and applies a detailed (resolution 50 × 50 m) reconstruction of the terrain in early medieval times (Figs. 1 and 2). This palaeo-DEM was largely constructed by a 'top-down' approach: removing all anthropogenic relief elements from a LiDAR ground level DEM (Van der Meulen et al., 2020). Additionally, the river channel position was reconstructed based on historical geographical and geological information, and the river bathymetry and proximal floodplain topography were restored using different interpolation methods aided by geological-geomorphological data (Van der Meulen et al., 2020). Hydraulic roughness values used in the modelling were specified considering relative terrain elevations and general insights regarding vegetation composition and early medieval land use (Van der Meulen et al., 2021). The five resulting landscape classes and associated roughness values (Manning's coefficient) were: river bed (n = 0.03), proximal floodplain (riparian vegetation on low banks and agriculture on high banks, n = 0.07), low distal floodplain (mostly grass, n = 0.04), high distal floodplain (mostly agriculture n = 0.05), and high ground (mostly forest, n = 0.1).

The model has a one dimensional-two dimensional (1D-2D) coupled set-up, with the main channels of the Rhine River and its distributaries in the delta schematised by 500-m-spaced 1D profiles and the floodplains discretised on a 2D rectangular grid with a resolution of 200 × 200 m. Flexible grid shapes are used along the model domain boundaries and along the transition from reworked to inherited floodplain. The hydrodynamic model was set up in HEC-RAS (v 5.0.3) using the full momentum equations to solve the system. To obtain representative palaeoflood input discharge time series, Van der Meulen et al. (2021) scaled the hydrograph of December 1925/January 1926 (Bomers et al., 2019a) measured at Andernach, Germany, since its shape is close to the average of modelled extreme flood waves of the Rhine River near Andernach (Hegnauer et al., 2014). The discharge of the tributaries Sieg, Ruhr and Lippe was simplified to constant input values of 250, 500 and 250 m^3/s, respectively.

For our purpose, we selected scaled hydrographs with peak discharges of 6000, 10,000 and 14,000 m^3/s (Fig. 6). A discharge wave of 14,000 m^3/s at Andernach results in a maximum discharge of 13,000 m^3/s downstream in the Netherlands due to the diffusion of the discharge wave, and a discharge partitioning of 4500 m^3/s routed northwards along the IJssel pathway and 8500 m^3/s westwards to the Waal-Nederrijn delta (Van der Meulen et al., 2021).

3.2. Adjustments in the IJssel divide breach area

For the purposes of this study, the palaeo-DEM was adjusted locally in the IJssel divide breach area (see Section 2), to restore the coversand ridge across the full breached trajectory (Fig. 7). These alterations were performed using ArcGIS software (ArcMAP 10.5). The parabolic shape of the reconstructed dunes of the coversand ridge is based on the dimensions and shape of the coversand dunes that LiDAR imagery reveals on either side of the IJssel breached zone. Further adjustment of the palaeo-DEM in the divide zone, is the implementation of the two

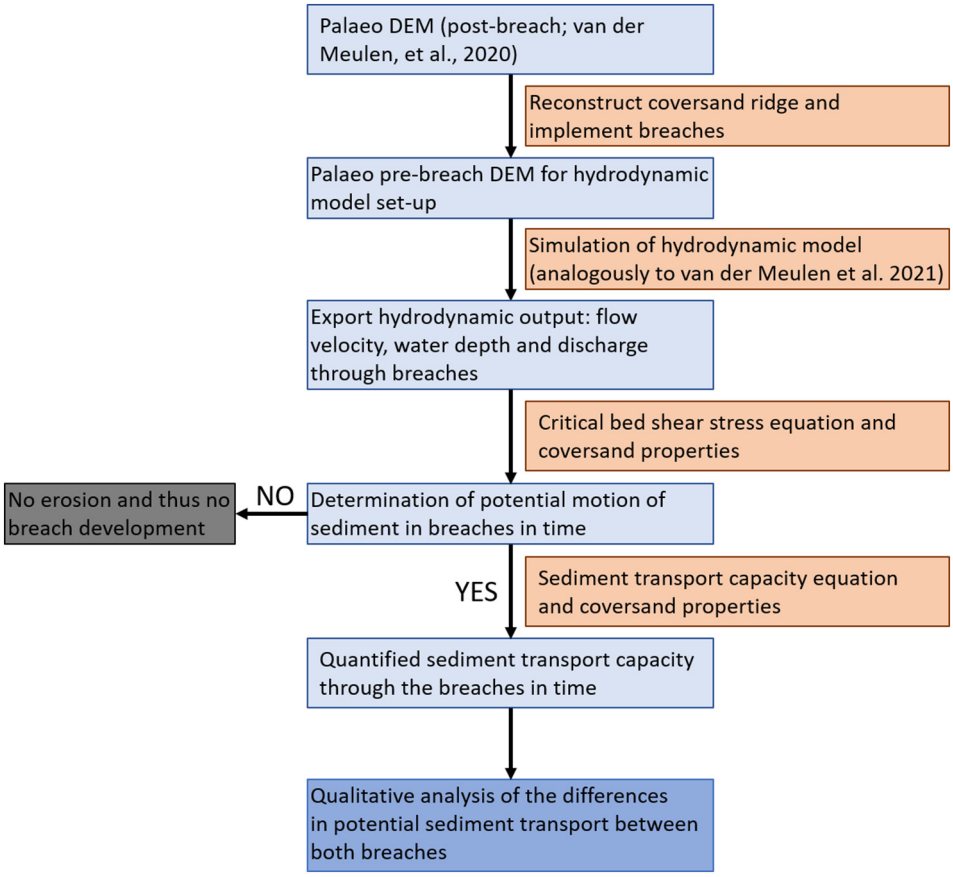

Fig. 5. Modelling flow chart.

breaches, with pre-defined width and depth. The prescribed dimensions were based on the current knowledge of the preserved breach near Voorst (see Section 2), and set to a breach depth of 2 m and a breach width of 50 m (Figs. 8 and 9). These dimensions would represents the breach channels in initial state, during their erosive formation process.

The roughness classification is altered at the locations of the coversand ridge breaches to conform with the non-cohesive sediments that were present (median grain size about 0.2 mm). We assigned the breaches a Manning's coefficient of 0.012, as according to Arcement and Schneider (1989) this corresponds to a sand channel with the flow being in upper regime. An upper regime applies if ripples and dunes are washed out by the forces of the flow, replacing it with a plane bed and antidunes, erosional chutes and pools which is typically the case during breach development (Arcement and Schneider, 1989).

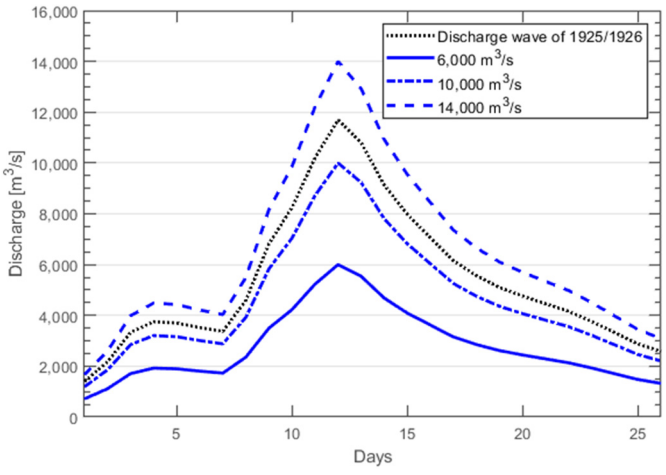

Fig. 6. Input hydrographs at the upstream boundary (between Andernach and Bonn) scaled on the 1925/1926 discharge wave.

Lastly, the modelling grid resolution was locally increased. The 200 × 200 m resolution used across the full modelling domain (see above) cannot accurately simulate the flood wave propagation through the breaches in the coversand ridges, which have a modelled width of 50 m. Two modifications were necessary. At the breach locations, the grid was refined to an average grid size of 10 × 20 m, allowing us to extract more accurate predictions of the local flow velocities and water depths in these breaches. Furthermore, the grid was modified such that flexible unstructured grid shapes are located along the coversand ridges, ensuring alignment of the grid with the natural elevation and more accurate calculation of its overtopping. The grid was only refined in the breached part of the divide, to keep computational time stays within reasonable bounds.

3.3. Coupled hydrodynamic-sediment transport model set-up

The hydrodynamic model is a large-area model, extending from upstream of Bonn, Germany, to the Betuwe and IJssel areas in the Netherlands (Fig. 1), of which the IJssel divide breach occurs in a fairly small section of this model domain (Fig. 2). Large-area hydrodynamic modelling is required to generate the flooding simulations and evaluate propagation into the divide region. Its output over the refined grids in the IJssel divide region was taken as input of a local sediment transport model (Section 3.3.1) and to analyse the results of the coupled hydrodynamic-sediment transport model in detail, and a graphic interface was set up (Section 3.3.2).

3.3.1. Local sediment transport model

To analyse breach scouring and sediment transport conditions, a morphostatic computation is performed, using a sediment transport

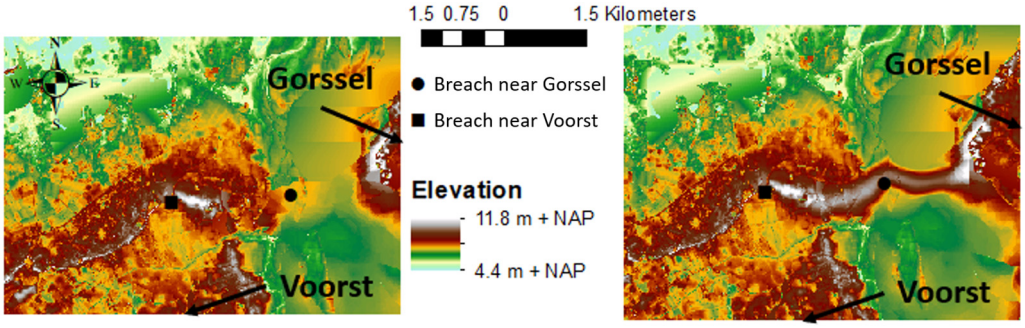

Fig. 7. Reconstructed coversand ridge connection in the northeastern part of the model domain. Left figure: After the breach of the coversand ridge; Right figure: Prior to the breach of the coversand ridge. Location is given in Figs. 1 and 2.

equation to assess potential conditions in the breach channels at selected moments during passing of a flood wave and for step wise increases of the breach channel depth. This allowed us to identify the differences in the sediment transport capacity of the two breaches. The morphostatic approach was chosen above modelling the breach development dynamically, as that would have been too computationally demanding and impractical as it may have required severe changes in the hydrodynamic modelling setup. The sediment transport model of Engelund and Hansen (1967) requires few input parameters and the equation of Engelund and Hansen (1967) is recommended for the computation of the total sediment load (suspended + bed load) of relative fine material. To obtain a quick insight into the morphological behaviour of the breaches, first the bed shear stress in the breaches is computed based on the hydrodynamic model output (Eq. (1)). If the threshold value for the start of motion is exceeded (computed with the critical bed shear stress, Eq. (2)), the flow is able to transport sediment and the breach is thus in an erosional phase. The actual and critical bed shear stress are computed using, respectively:

$$\tau = \rho g[\overline{u}/C]^2 \tag{1}$$

$$\tau_{cr} = \theta_{cr}(\rho_s - \rho)gD_{50} = 0.16\ \mathrm{N/m^2} \tag{2}$$

With:

$$\theta_{cr} = \frac{0.14}{D_*^{0.64}} = 0.048 \tag{3}$$

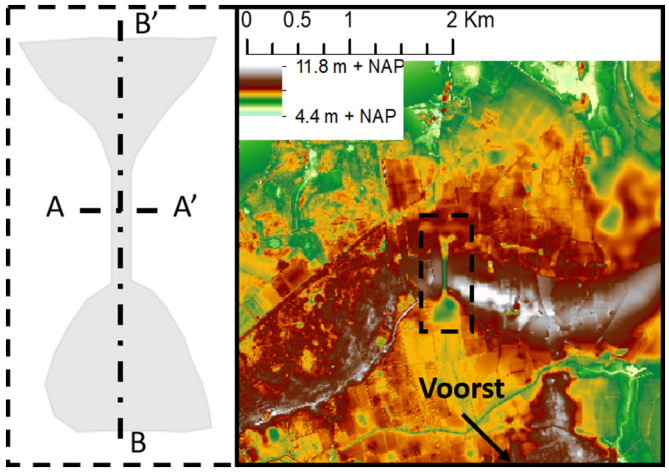

Fig. 8. Location of the cross section at the centre of the breaches where the sediment transport capacities are computed (breach near Voorst). Location is given in Figs. 1 and 2.

$$D_* = D_{50}\left[(\rho_s/\rho - 1)g/\nu^2\right]^{1/3} = 5.3 \tag{4}$$

In these equations, D_* is the dimensionless grain size parameter, with the median grain size of the sediment D_{50}=210 μm, the sediment density ρ_s=2650 kg/m^3, the water density ρ=1000 kg/m^3, the gravitational acceleration g=9.81 in m/s^2, the viscosity of water $\nu = 1{*}10^{-6}$ in m^2/s. θ_{cr} is the Shields critical value at initiation of motion in terms of the grain size parameter (D_*) (Shields, 1936; van Rijn, 1993) and τ_{cr} is the critical bed shear stress in N/m^2. τ is the actual bed shear stress in N/m^2, with the depth-averaged flow velocity $\overline{u}$ in m/s, C is the Chézy coefficient in $m^{0.5}/s$, determined using the equation $C = h^{1/6}/n_{Manning}$, in which h is the water depth in m and $n_{Manning}$= 0.012.

If the breach is in an erosional phase, the potential sediment transport capacity through the breaches is computed, using a simplified version of the sediment transport equations of Engelund and Hansen (1967). In general, sediment transport equations are of the form:

$$s = m\overline{u}^n, \quad with \quad m = \frac{0.05}{\sqrt{g}C^3\Delta^2 D_{50}} \tag{5}$$

In this equation, s is the sediment transport in $m^3/s/m$, n is equal to 5 because the conditions of the equation of Engelund and Hansen (1967) apply, and $\Delta = [\rho_s - \rho]/\rho$.

The sediment transport capacity is computed at the cross section of the breaches (A-A′ in Figs. 8 and 9) using Eq. (5). The initial conditions (i.e., the mean grain diameter, breach width and breach depth) of the two breaches were assumed to be equal as geological data do not suggest any differences (Cohen et al., 2009). Therefore, it is possible to interpret the relative differences between the quantified potential sediment transport capacities in both breaches qualitatively. The differences between the quantified potential sediment transport capacities during a flood wave can then be translated to a scenario sketch of what could have taken place in both breaches during the avulsion-by-annexation process.

3.3.2. Interface set-up for breach development analysis

An interface is set up to analyse the potential breach development in both locations (Fig. 10). This interface consists of three parts. The upper two figures represent the direct hydrodynamic output in the two breaches at timestep 't'. The middle figure shows the discharge in time through both breaches and the lower figure shows the computed potential sediment transport capacity through the breaches during the flood wave.

3.4. Sensitivity analysis

To test the robustness of our main findings, a sensitivity analysis is performed. Breaches with different widths and depths are implemented in the palaeo-DEM. We focused on the differences in the potential sediment transport rates between both breaches under different initial

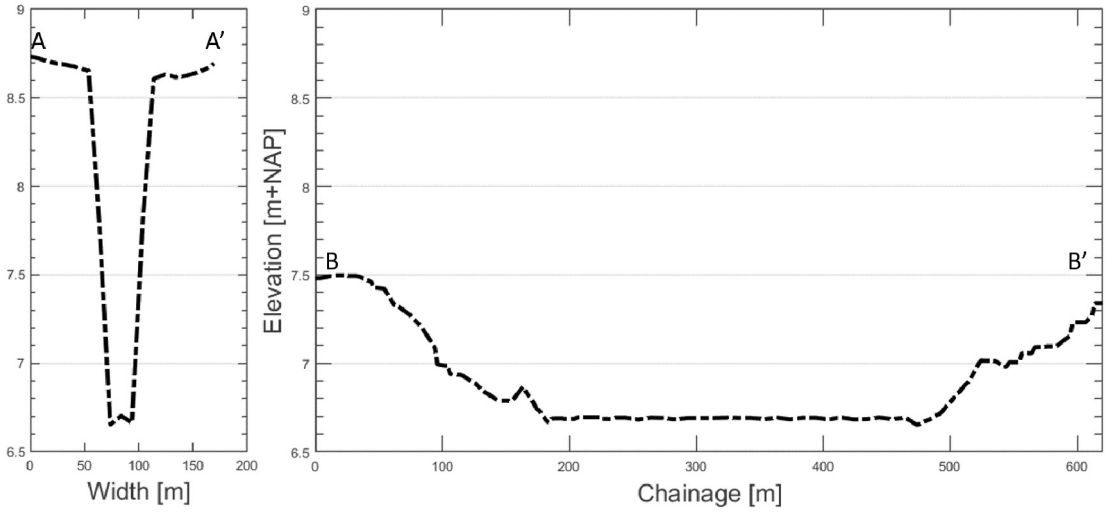

Fig. 9. Bathymetry of the cross section and longitudinal section in the breaches where the sediment transport capacities are computed (breach near Voorst).

breach dimensions and for different upstream discharge waves with a peak value of 6000 and 10,000 m^3/s.

Scenarios with a breach depth of half and double the original depth are constructed (Table 1). Besides this, the breach width is increased by a factor two resulting in a breach width of 100 m. Lastly, two scenarios are set up in which both breaches have different dimensions. These scenarios are set up to gain insight in the potential breach development of the two breaches at different stages of the breach development process. The various dimensions constructed for the sensitivity analysis are shown in Table 1.

4. Results

4.1. Hydrodynamic conditions

The hydrodynamic simulation with an upstream peak discharge of 14,000 m^3/s results in a discharge distribution of approximately 4500 m^3/s on the IJssel floodplain (Fig. 11). The geographical situation forces the flood wave to flow through the incipient valley topography. Because of the relatively low bed levels of this valley compared to the surrounding terrain, the flood flows towards the breach near Gorssel (Fig. 12). As a result, this breach becomes active approximately five hours before the breach near Voorst actively discharges water (Fig. 12). The geographical situation of the IJssel floodplain thus directly influenced the hydrodynamic conditions in both breaches. To what extent this is affected by the choices in the palaeo-DEM construction is discussed in Section 5.1.3 in more detail.

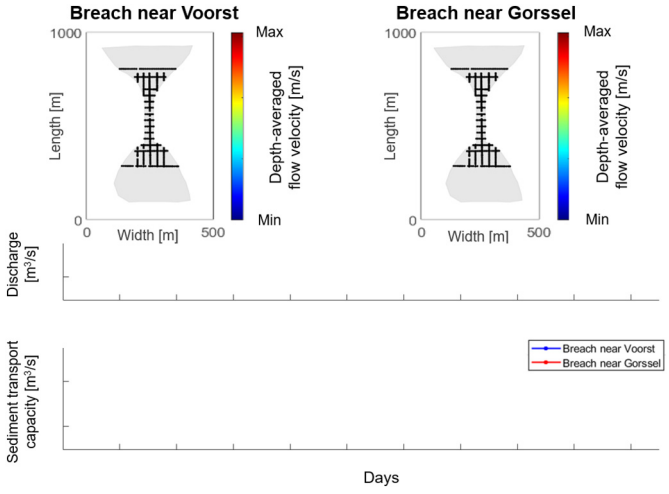

Fig. 10. Interface showing plan view of the flow velocities in the two breaches (top), discharge in time (middle), and sediment transport capacity in time (bottom).

The breach near Gorssel is subject to larger depth-averaged flow velocities than the breach near Voorst for two reasons (Fig. 12). First, before the flood wave reaches the breach near Voorst, the flood wave has to deflect to the West resulting in a lowering of the flow velocities. Second, the flood wave diffuses and dissipates farther downstream, decreasing the flow velocities.

4.2. Critical bed shear stress

To get a first insight into the morphological behaviour of the two breaches during the flood wave, the critical bed shear stress of the coversand is determined and compared to the actual bed shear stress in the breaches. The threshold value for putting sediment into motion is exceeded just after the breaches start to discharge water, when the hydrodynamic conditions for sediment transport are least favourable because of the still relatively low water depths and flow velocities. Thus, the breaches will be in an erosional phase during the entire flood wave, when hydrodynamic conditions are more extreme than at the start (Fig. 14).

Both breaches erode during the flood wave, but the breach near Gorssel is in an erosional phase earlier in time and is therefore expected to expand earlier (Figs. 13 and 14). This is in line with the propagation of the flood wave as shown in Section 4.1.

4.3. Potential sediment transport capacity

Because the potential sediment transport capacity is a function of the flow velocity (Eq. (5)), the breach near Gorssel shows higher

Table 1
Dimensions of the breaches in the coversand ridges for the static modelling approach in the different scenarios for the sensitivity analysis.

Breach near Voorst		Breach near Gorssel	
Width [m]	Depth [m]	Width [m]	Depth [m]
Equal dimensions			
50	1	50	1
50	2	50	2
50	4	50	4
100	4	100	4
Different widths			
50	4	100	4
100	4	50	4

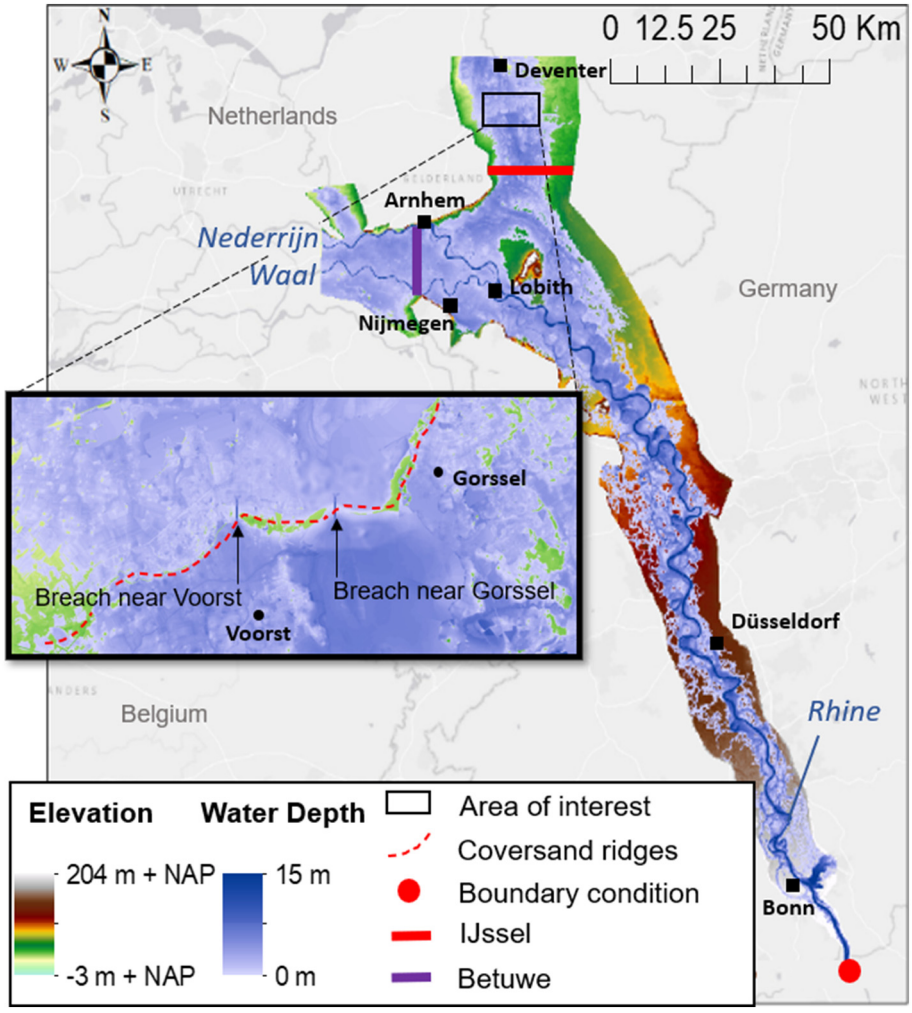

Fig. 11. Inundation of the full modelling domain during a flood wave with a peak discharge of 14,000 m^3/s.

potential sediment transport rates during the flood wave (Fig. 15). With equally large pre-defined breaches in the coversand ridge, the breach near Gorssel has a potential sediment transport capacity which is twice as large as of the breach near Voorst. Thus, with the assumption that the flood wave transports an equal amount of sediment at the incoming flow funnel of both breaches, resulting in equal initial conditions, the breach near Gorssel is expected to expand faster.

4.4. Sensitivity analysis

A sensitivity analysis is performed in which the parameters breach width, breach depth and peak value of the upstream discharge wave are varied. This section elaborates on these results.

4.4.1. Equal breach dimensions

The simulations performed for the sensitivity analysis imply that, under equal initial conditions for both breaches, the breach near Gorssel shows higher potential sediment transport capacity rates in time relative to the breach near Voorst for all parameter settings (Fig. 16). Besides this, the breach near Gorssel will always start to actively discharge water and transport sediment earlier in time. Both factors indicate that the breach near Gorssel is expected to expand faster under equal initial conditions. Changing the parameters breach width, breach depth and upstream peak discharge, does not change the predicted differences in sediment transport rates between the two breaches. This indicates that, for equal initial breach dimensions, the breach near Gorssel develops faster compared to the breach near Voorst regardless of the initial parameter values.

Furthermore, the potential sediment transport rates of both breaches first increase with an increasing initial breach depth, while these rates will eventually decrease with both an increasing initial breach depth and breach width (Fig. 16). The relative difference of potential sediment transport capacity between both breaches, on the other hand, increases. With a small initial breach (50 m × 1 m) the potential sediment transport capacity of the breach near Voorst is approximately 0.4–0.45 times less than the breach near Gorssel (depending on the peak discharge; Fig. 16A and B). With the largest initial breach (100 m × 4 m) this ratio decreases to approximately 0.08–0.11 (Fig. 16G and H). In other words, the larger the initial breach at both locations, the larger the advantage of the breach near Gorssel. However, note that the presented potential sediment transport rates are computed using constant breach dimensions during the entire simulation. In reality, the breach grows during the period of erosion, resulting in a decrease of the water depth and flow velocity which in turn decreases the energy gradient of the breach.

4.4.2. Different breach dimensions

Lastly, several scenarios are simulated to gain insight into the breach development of the two breaches at different stages of the breaching process. A scenario with an initially wider breach near Gorssel (100 m × 4 m) compared to the breach near Voorst (50 m × 4 m) is simulated with three different flood waves (6000, 10,000 and 14,000 m^3/s). All flood waves result in higher sediment transport capacity rates at the

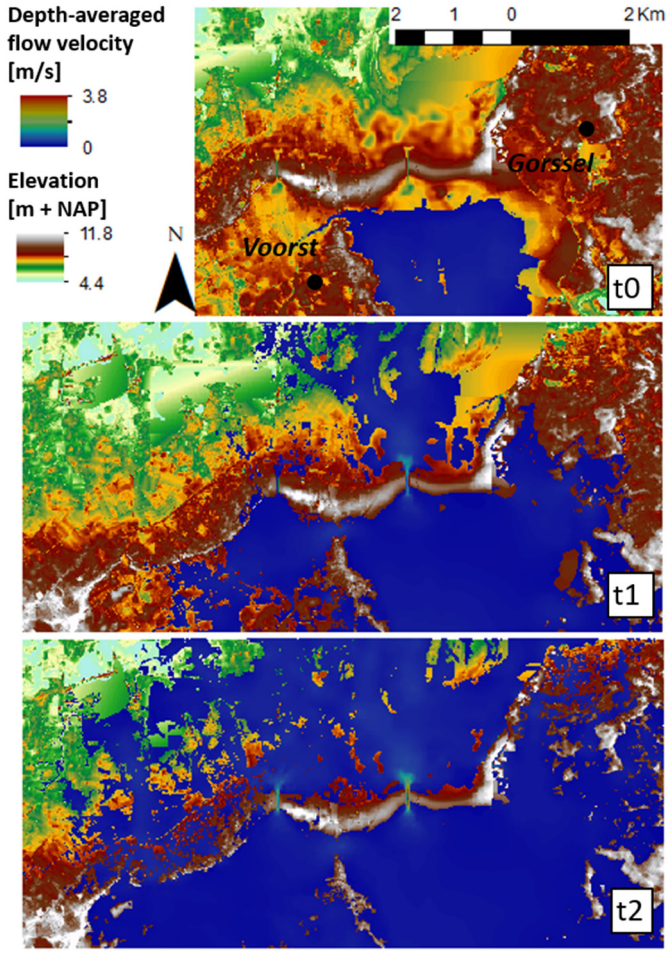

Fig. 12. Flood wave propagation at the breach locations. t0 is just before the flood wave reaches the breach near Gorssel, t1 is 12 h after t0 and t2 is 24 h after t0. Location is given in Figs. 1 and 2.

breach near Gorssel relative to the breach near Voorst (Fig. 17A, B and C). The potential sediment transport capacity ratio between both breaches again shows an advantage for the breach near Gorssel. Although the differences are less extreme, the breach near Gorssel is expected to develop faster than the breach near Voorst. Besides this, a relatively small upstream flood wave of 6000 m^3/s shows a larger potential sediment transport ratio, indicating that in later times, the breach near Gorssel will develop more than the breach near Voorst because of smaller subsequent floods.

A scenario with an initially wider breach near Voorst (100 m × 4 m) compared to the breach near Gorssel (50 m × 4 m) is also simulated. These simulations resulted in extreme differences in potential sediment transport ratios (Fig. 17D and E), with the breach near Gorssel being able to transport approximately 27–55 times more than the breach near Voorst. This difference in sediment transport ratios will even be larger for an initially wider breach near Voorst, as flow velocities will be lower resulting in a further reduction of the transport ratio. The smaller breach near Gorssel is expected to develop faster than the breach near Voorst, eventually being equally large. From a scenario with equally large dimensions is known that the breach near Gorssel will develop faster (Fig. 16G and H). From the morphostatic modeling, it can thus be concluded that the breach near Gorssel is expected to always develop faster, independent of the initial breach dimensions. We note that upgrading to a morphodynamic modelling setup, avoiding the crude stepwise prescription of breach channel dimensions, might give more detailed insight in the development of the two competing breaches.

5. Discussion

5.1. Suitability of the terrain reconstruction

5.1.1. Reconstructed divide topography

Coversand ridge topography was restored across the IJssel divide breach area to have a pre-breach palaeo-DEM (Fig. 7). This reconstructed divide topography projected the dimensions and shapes of coversand idges still present east and west of the current IJssel River system (e.g., mapping such as in Cohen et al. (2009)), based on expert judgement and ad-hoc interpolation decisions when operating the GIS software. The restoration was performed over limited width of the study area. The breach locations through the restored divide were independently positioned, i.e., not resulting from saddle elevations of the interpolated ridge. It is possible that the divide had a narrower crest (compare areas to west in Fig. 7) than considered for our reconstructed section, but such nuance would have minimal effect on the potential sediment transport and initial erosion results, as the chosen crest width does not influence the breach locations.

The choice of crest elevation was based on values picked from the surrounding preserved coversand ridges, and set to an equal height along the whole crest of the reconstructed coversand ridge. Crest width and height choices together thus represent a best guess

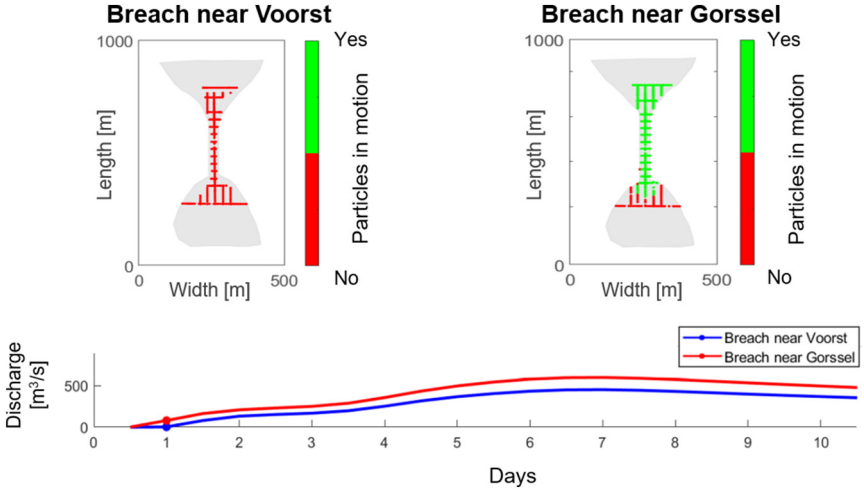

Fig. 13. Particles in motion 't_1'.

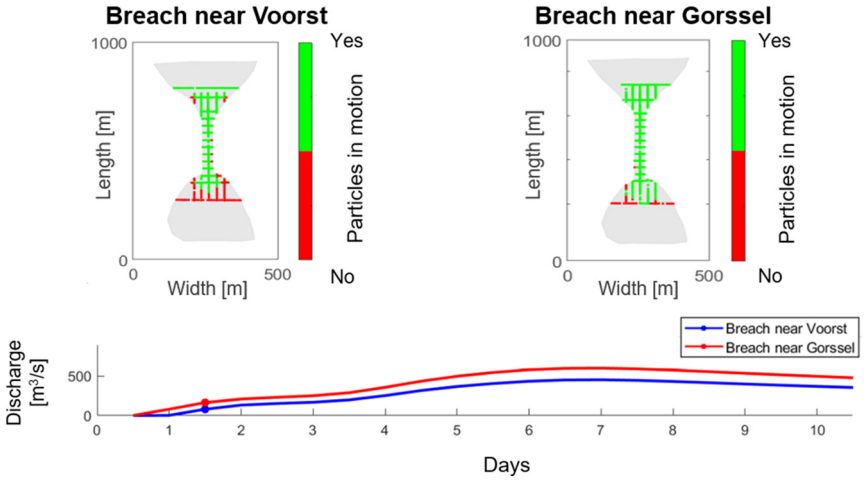

Fig. 14. Particles in motion 't_2'.

smoothed shape of a coversand ridge, where in reality, the eroded ridge will have shown local height and width variations. The choices of ridge reconstruction do matter for the modelling of overflow, which at a certain water level would first occur at a single location, while at other locations it would not occur yet. Whether a smoothed or a more varied restoration of missing topopgrahy is adopted, in both cases it should be noted that the overflow locations that the modelling produces (Fig. 11) are co-affected by grid layout choices (see Section 3.1). Such also holds for locations where breach erosion initiated, i.e., an overflow location transformed into a breach location.

Independent from local reconstructed divide crest width and height, the stepped morphostatic modelling prescribed initial breach channel depths of 1 and 2 m at the two predetermined breach locations. The crest heights of the surrounding coversand ridges deviated at maximum 0.5 m, meaning that water always started to flow through the breaches before overflow of the surrounding coversand ridges started to occur. For this reason, the reconstructed crest height does not affect the results.

5.1.2. The location of the breach near Gorssel

From geological mapping and dating (see Section 2) the location of the breach near Voorst could be determined accurately (Fig. 7), but that of the breach near Gorssel can only be estimated, as widening and lateral migration of subsequent rivers washed out most of the initial topography. In the erosion and sediment transport capacity calculations of the competing breach channels, a fixed pre-scribed position of the breach near Gorssel was considered. To test whether the results are sensitive to the precise arbitrary location, an additional coupled-modelling scenario was constructed in which a farther eastward location of the breach was considered (Fig. 18), with the default values for breach width (50 m) and breach depth (2 m). The maximum depth-averaged flow velocity of the breach near Gorssel located at the original location and the breach constructed for validation were, respectively, 7.34 m/s and 7.11 m/s. This is a deviation of approximately 3%. Changing the location of the breach near Gorssel did not affect the hydrodynamic conditions in the breach near Voorst. Thus, differences in computed flow

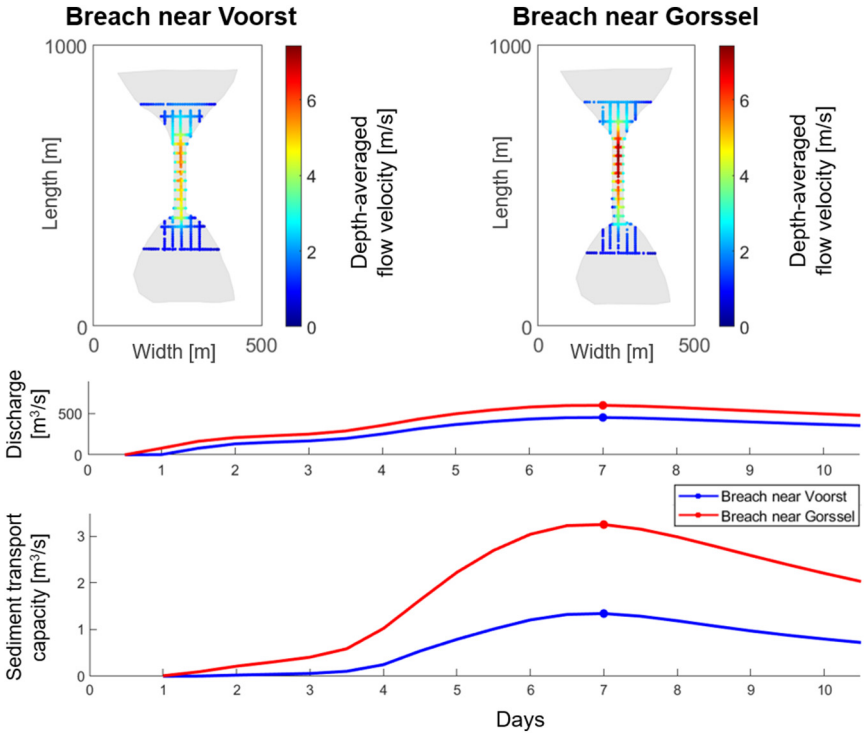

Fig. 15. Hydrodynamic-sediment transport model for the case with a breach depth of 2 m, breach width of 50 m and a discharge wave of 14,000 m^3/s at Andernach.

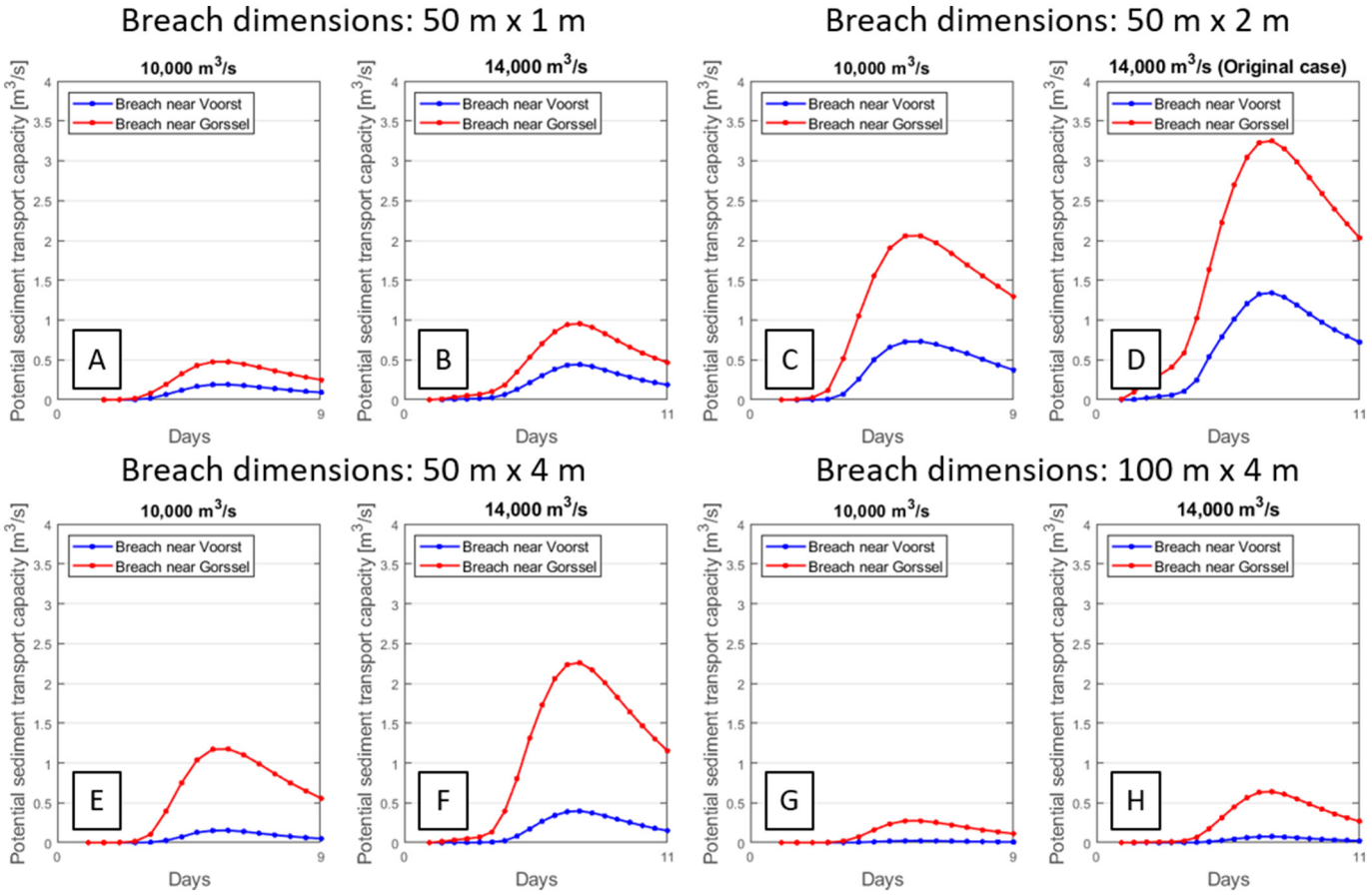

Fig. 16. Potential sediment transport capacity in both breaches under equal initial conditions.

velocities in the two breaches are insensitive to the exact location assigned to the breach near Gorssel. Because potential sediment transport capacity is a function of depth-averaged flow velocity mainly, that result is also insensitive.

5.1.3. Palaeo-DEM quality North and South of the IJssel breached divide

South (upstream) and north (downstream) of the restored IJssel divide, the palaeo-DEM shows topographic lows inherited from the source palaeo-DEM (Fig. 7). In part, this is realistic topography as local drainage networks were present prior to establishment of the river (e.g., Vermeulen and Haveman (2008)) that merged into 'brook valleys' (Fig. 4A), and that in the corridor used by the avulsing IJssel River would have been overwhelmed and reworked (Makaske et al., 2008; Cohen et al., 2009). The widths of these valleys would have been narrower than the topographic low features in the palaeo-DEM. The cause of this is that to create the palaeo-DEM, IJssel-affected morphology was stripped and replaced with a minimum elevation based on morphological remnants including the preserved brook valley floors and peat growth (Van der Meulen et al. (2020) and sources therein), and no further steps of topping up parts of the corridor with patchy coversand relief were undertaken. Issues that prevented doing so in the previous study were (i) the arbitrary nature of demarcating specific boundaries between lost cover sand relief and lost brook valley lows, and (ii) the target age of the palaeo-DEM being 800 CE, a first moment after the initial breaching of this study with an avulsion belt established in the area (e.g., Fig. 4B), washing out the coversand relief. The current study, made a begin of restoring the coversand topography in the IJssel part of the Lower Rhine palaeo-DEM (Fig. 2), but only for the divide reach. In areas north and south of the divide, no further local, isolated coversand elements were restored.

Improved restoration of brook-dissected coversand topography in the palaeo-DEM would reduce water depths in the ponding floodplain area south of the divide and may modestly affect flow routing towards the two breaches and improve realism of the simulation, but is not regarded to affect the main findings regarding respective breach channel flow velocities and erosion potential. Improved restoration of coversand topography north of the divide would modestly alter run out pathways to this newly annexed part of the floodplain, but not majorly change the erosive capacity of the breach channels in the divide area properly.

5.2. Uncertainty in hydraulic modelling parameterisation

5.2.1. Hydraulic geometry of the breaches

The considered breaches are a schematic representation of reality, representing a situation of the Rhine and IJssel floodplain approximately 1300–1700 years ago. Therefore, the breach dimensions and properties are only best guess reconstructions from geological mapping and dating information (see discussion in Van der Meulen et al. (2020)). In this study, trapezoidal dimensions are implemented, while other studies consider different shapes like rectangular (Singh and Scarlatos, 1988), triangular (Fread, 1984) and parabolic shapes (Brown and Rogers, 1981). The flow velocities mostly determine the erosion capacities that mainly depend on the upstream flood wave and the cross-sectional area of the breach rather that its shape. So, it is expected that using different breach shapes will not significantly affect the qualitative analysis of the quantitative results.

This research only considered the cohesion of loosely packed sediment. In reality, this sediment may locally have been more cohesive because of the soil formation throughout the thousands of years and the vegetation that would have increased the cohesion from the roots.

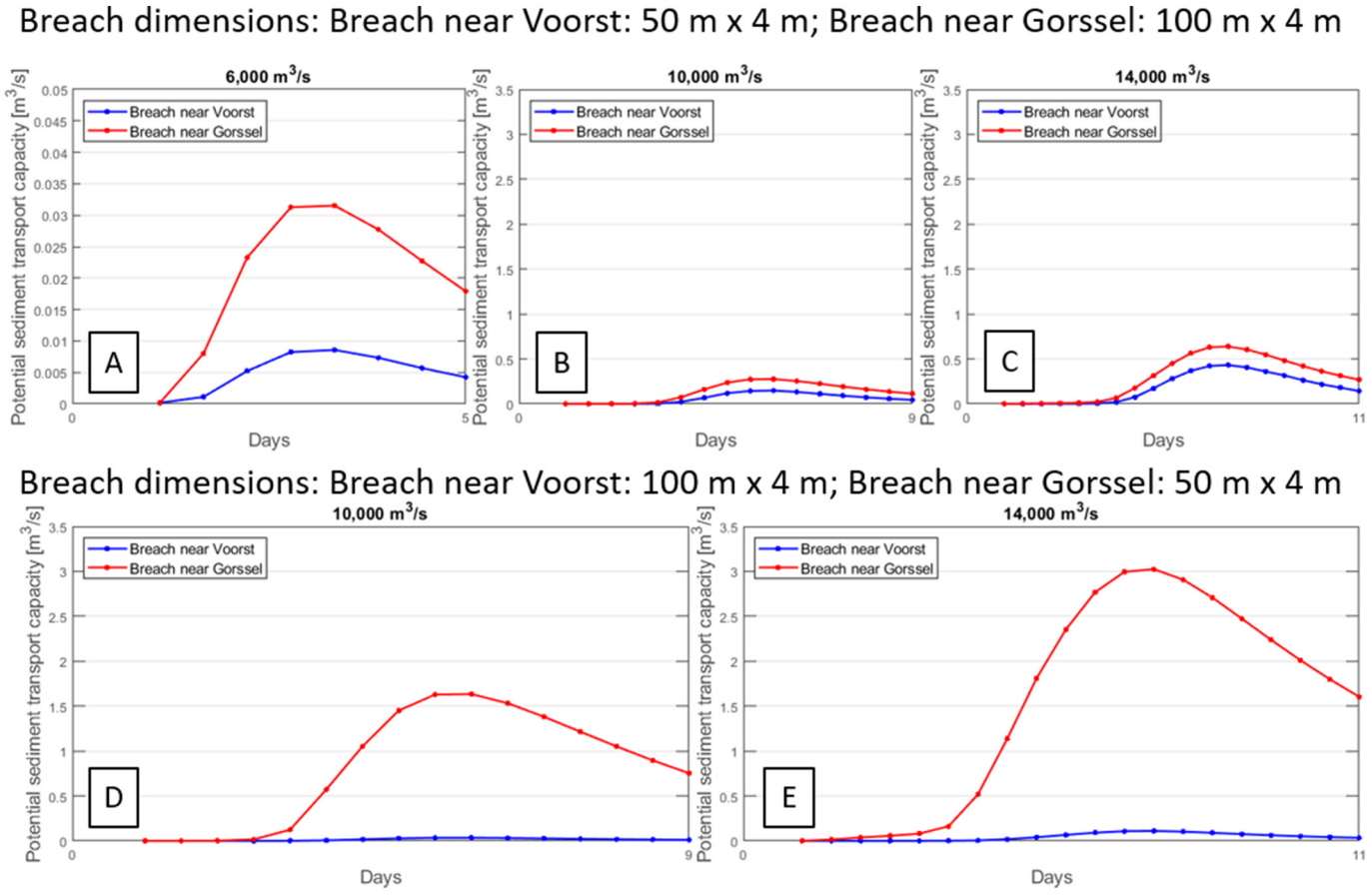

Fig. 17. Potential sediment transport capacity in both breaches under different initial conditions. Note that the potential sediment transport capacity of sub-fig. A is scaled differently on the y-axis than the other figures due to the relatively low potential capacity rates.

This again does not have an impact on the qualitative analysis because only situations were considered in which the vegetation was already washed away at the breach location and only non-cohesive sediment was left. The increase in cohesion caused by the vegetation would have had an impact on the timing of the erosion initiation of the crest, which is outside the scope of this research.

5.2.2. Hydrodynamic-sediment transport model set-up

The hydrodynamic model has a 2D grid on the floodplains. At the breach locations, the grid was constructed manually such that it is aligned with the coversand ridges at the areas of interest. The manual refinement resulted in a so-called unstructured grid with various grid cell shapes at the breach locations. The model output was within the boundaries of observed geological data, but could not be validated with in-situ measurements because the erosion and eventually breaching of the coversand ridges and avulsion of the IJssel River took place during a large palaeoflood with a magnitude exceeding the maximum discharge in instrumental record (Van der Meulen et al., 2021). Deploying other grid refinement methods (i.e., different grid shapes or resolutions) could potentially lead to different results (Bomers et al., 2019c). However, it is expected that as long as the grids for both breach channels are refined according to the same method, the respective results obtained for each breach will not be qualitatively different (the breach near Voorst will not be favoured above the breach near Gorssel, just because of re-gridding). In our study, it was not possible to deploy multiple grid refinement methods because of computational time and software limits.

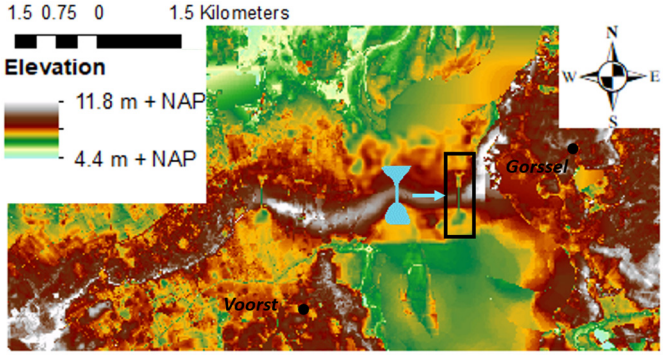

Fig. 18. Alternatively positioned breach location near Gorssel considered during the sensitivity analysis (compared to Fig. 7) with the original breach location given in blue. Location of the map is given in Figs. 1 and 2.

The unstructured grid aligned along a part of the coversand ridge has a major impact on the discharge distribution on the floodplain. The grid is only aligned at the area of interest, but west and east of the 2D grid a structured and coarser 200 m × 200 m grid is present. These cells may overlay the entire coversand ridge and consequently cause the hydrodynamic model to compute water levels on the downstream side of the coversand ridge because of the lower elevation, while in reality no water has overflown the coversand ridge yet. This research is interested in the differences between both breaches in the coversand ridges under various conditions. In reality this means that the water level and thus the pressure caused by the flood wave would be larger than depicted here. Therefore, the breaches would probably suffer higher flow and erosion velocities. However, it is expected that a better aligned grid throughout the model domain only has an effect on the quantitative results of the interaction between the two developing breaches.

Furthermore, we used a so-called morphostatic modelling approach to compute the potential erosion development without the implementation of a morphodynamic model. This means that the feedback between the growing breach and the flow is not included. The development of the breaches in time can only be sketched by an interpretation of the morphostatic model results. A sophisticated morphodynamic model can give more insight in the interaction of both breaches during the different breach development stages. However, because the morphological development of the two breaches is highly uncertain and cannot be validated, a morphostatic approach is sufficient for this study, i.e., to study whether the floods were strong enough to make the two breaches grow and whether and why one of the two breaching candidates was favoured.

5.3. Sediment transport model

Conforming to geological observations (Section 2), a sediment diameter of 210 μm was used for the sediment transport equation and for the determination of the roughness in the breaches in the hydrodynamic model. It is assumed that this represents the median diameter of the sediment and that the sediment is uniformly distributed. If the median grain size of the sediment is, for example, larger than the considered median sediment diameter, the Manning's coefficient would be larger. A higher roughness in the breaches causes lower flow velocities locally. Both the median grain size as well as the flow velocity affect the sediment transport capacity. A lower flow velocity and larger grain size will result in less potential sediment transport capacity. In this study, the sediment distribution was equal along the coversand ridges. So, the decrease in potential sediment transport capacity will occur in both breaches and will not affect the qualitative findings.

6. Conclusion

In this research, a significant step is made in connecting geomorphological reconstruction of stages of river establishment to numerical modelling of formative events. The work shows that a palaeoflood hydrodynamic model can be used for setting up a local sediment transport model, and that such is relevant for analysing the early stages of a major avulsion in the Rhine delta, the Netherlands: that of the IJssel River in early medieval times, establishing the river network still functioning today.

We focused on modelling the flood-induced initial breaching of a drainage divide constituted by a coversand ridge of pronounced height and continuity between Voorst and Gorssel, across what now is channel and floodbed of the IJssel River. The hydrodynamic conditions and sediment transport rates in two competing breaches were examined for various upstream discharge waves. It was found that the breach near Gorssel, positioned at the eventual location of the IJssel River, was subject to significantly higher depth-averaged flow velocities and sediment transport rates compared to the breach near Voorst. Furthermore, the flood wave reaches the breach near Gorssel some five hours earlier than it reaches the breach near Voorst. These two findings explain and subscribe to the notion that the breach near Gorssel expanded earlier and faster and thus why the IJssel River established at this breach location. Simultaneously it explains that the breach near Voorst has functioned only briefly, essentially just during one flood, allowing it to be preserved.

Despite the uncertainties related to the reconstruction of breach dimensions and the relatively simple modelling approach, the conditions allowing the breach to expand were intrinsically more favourable for the breach near Gorssel, as shown by varying initial breach dimensions and upstream discharge waves in the sets of simulation scenarios. In tandem with the flood modelling for the Lower Rhine full model domain (Van der Meulen et al., 2021), the hydrodynamic-morphostatic coupled approach deployed in this paper, provides quantitative argumentation for large floods to have triggered the avulsion of the IJssel River, through the mechanisms of local breach initiation and quickly resolved interbreach competition. This shows that hydrodynamic models can be effectively used to gain insight in past fluvial processes to understand river landscape evolution.

Declaration of competing interest

The authors declare that they have no known competing financial interests or personal relationships that could have appeared to influence the work reported in this paper.

Acknowledgements

This research is supported by the Netherlands Organisation for Scientific Research (NWO, Project 14506) which is partly funded by the Ministry of Economic Affairs and Climate Policy. Furthermore, the research is supported by the Ministry of Infrastructure and Water Management and Deltares.

References

Arcement, G.J., Schneider, V.R., 1989. Guide for selecting Manning's roughness coefficients for natural channels and floodplains. United States Geological Survey Water-Supply, 2339. https://doi.org/10.3133/wsp2339.

Benito, G., Thorndycraft, V., 2005. Palaeoflood hydrology and its role in applied hydrological sciences. J. Hydrol. *313*, 3–15. https://doi.org/10.1016/j.jhydrol.2005.02.002.

Bomers, A., Schielen, R. M. J., & Hulscher, S. J. M. H. (2019a). Application of a lower-fidelity surrogate hydraulic model for historic flood reconstruction. Environ. Model. Softw., *117*, 223–236. doi:https://doi.org/10.1016/j.envsoft.2019.03.019.

Bomers, A., Schielen, R. M. J., & Hulscher, S. J. M. H. (2019b). Consequences of dike breaches and dike overflow in a bifurcating river system. Nat. Hazards, *97*, 309–334. doi:https://doi.org/10.1007/s11069-019-03643-y.

Bomers, A., Schielen, R. M. J., & Hulscher, S. J. M. H. (2019c). The influence of grid shape and grid size on hydraulic river modelling performance. Environ. Fluid Mech., *19*, 1273–1294. doi:https://doi.org/10.1007/s10652-019-09670-4.

Brown, R.J., Rogers, D.C., 1981. BRDAM Users Manual. Technical Report Water and Power Resources Services, U.S. Department of Interior.

Burge, L., 2006. Stability, morphology and surface grain size patterns of channel bifurcation in gravel–cobble bedded anabranching rivers. Earth Surf. Process. Landf. *31*, 1211–1226. https://doi.org/10.1002/esp.1325.

Busschers, F.S., Kasse, C., Balen, R.T., Vandenberghe, J., Cohen, K.M., 2007. Late Pleistocene evolution of the Rhine-Meuse system in the southern North Sea basin: imprints of climate change, sea-level oscillation and glacio-isostacy. Quat. Sci. Rev. 26, 3216–3248. https://doi.org/10.1016/j.quascirev.2007.07.013.

Cohen, K.M., Lodder, Q.J., 2007. Paleogeografie en veiligheid tegen overstromen. RIZA report 2007.016. Rijkswaterstaat.

Cohen, K.M., Stouthamer, E., Hoek, W.Z., Berendsen, H.J.A., Kempen, H.F.J., 2009. Zand in Banen: zanddieptekaarten van het Rivierengebied en het IJsseldal in de provincies Gelderland en Overijssel. Provincie Gelderland & Universiteit Utrecht.

Cohen, K.M., Stouthamer, E., Pierik, H.J., Geurts, A.H., 2012. Digitaal basisbestand paleogeografie van de rijn-maas delta / rhine-meuse delta studies' digital basemap for delta evolution and palaeogeography. Dept. Physical Geography. Utrecht University. https://doi.org/10.17026/dans-x7g-sjtw Digital Dataset. dans.

Cohen, K.M., Toonen, W.H.J., Weerts, H.J.T., 2016. Overstromingen van de Rijn gedurende het Holoceen: relevantie van de grootste overstromingen voor archeologie van het Nederlandse rivierengebied. Technical Report 1209091. Deltares.

Engelund, F., Hansen, E., 1967. A Monograph on Sediment Transport in Alluvial Streams. Teknisk Forlag, Copenhagen, Denmark.

Ente, P., 1971. Sedimentary geology of the Holocene in Lake IJssel region. Geol. Mijnb. 50, 373–382.

Erkens, G., 2009. Sediment dynamics in the Rhine catchment. Ph.D. Thesis. Netherlands Geographical Studies, p. 388.

Erkens, G., Hoffmann, T., Gerlach, R., Klostermann, J., 2011. Complex fluvial response to Late glacial and Holocene allogenic forcing in the Lower Rhine Valley (Germany). Quat. Sci. Rev. 30, 611–627. https://doi.org/10.1016/j.quascirev.2010.11.019.

Erkens, G., Toonen, W.H.J., Cohen, K.M., Prins, M.A., 2012. Unravelling mixed sediment signals in the floodplains of the Rhine catchment using end member modelling of grain size distributions. Extended Abstract. ICFS10, Leeds, UK, pp. 109–110.

Fread, J. N., D. L. Wetmore (1984). DAMBRK: The NWS dam break flood forecasting model. Technical Report National Oceanic and Atmospheric Administration.

Gouw, M., Erkens, G., 2007. Architecture of the Holocene Rhine-Meuse delta (The Netherlands): a result of changing external controls. Netherlands J. Geosci. 86.

Groothedde, M., 2010. De 'nieuwe' IJssel. Wat vertellen de geschreven bronnen en archeologische vondsten? Historisch Jaarboek voor Gelderland 101, 7–26.

Hajek, E.A., Edmonds, D.A., 2014. Is river avulsion style controlled by floodplain morphodynamics. Geology 42, 199–202. https://doi.org/10.1130/G35045.1.

Hajek, E., Wolinsky, M., 2012. Simplified process modeling of river avulsion and alluvial architecture: Connecting models and field data. Sediment. Geol. 257–260, 1–30. https://doi.org/10.1016/j.sedgeo.2011.09.005.

Harbers, P., Mulder, J.R., 1981. Een poging tot reconstructie van het rijnstelsel in het oostelijk rivierengebied tijdens het holoceen, in het bijzonder de romeinse tijd. Geografisch Tijdschrift 15, 404–421.
Hegnauer, M., Beersma, J.J., van den Boogaard, H.F.P., Buishand, T.A., Passchier, R.H., 2014. Generator of Rainfall and Discharge Extremes (GRADE) for the Rhine and Meuse basins. Final report of GRADE 2.0. Technical Report. Deltares Delft, The Netherlands ISBN:9789036914062.
Hesselink, A., 2002. History makes a river: morphological changes and human interference in the river Rhine, The Netherlands. Ph.D. Thesis. Netherlands Geographical Studies, p. 292.
Jansma, E., 2020. Hydrological disasters in the nw-european lowlands during the first millennium ad: a dendrochronological reconstruction. Neth. J. Geosci. 99. https://doi.org/10.1017/njg.2020.10.
Kalweit, H., Buck, W., Felkel, K., Gerhard, H., van Malde, J., Nippes, K.R., Ploeger, B., Schmitz, W., 1993. Der Rhein unter der Einwirkung des Menschen–Ausbau,Schiffahrt, Wasserwirtschaft. Internationale Kommission für die Hydrologie desRheingebietes (CHR/KHR).
Kleinhans, M. G., Jagers, H. R. A., Mosselman, E., & Sloff, C. J. (2008). Bifurcation dynamics and avulsion duration in meandering rivers by one-dimensional and three-dimensional models. Water Resour. Res., 44. doi:https://doi.org/10.1029/2007WR005912.
Kleinhans, M.G., Weerts, H.J.T., Cohen, K.M., 2010. Avulsion in action: Reconstruction and modelling sedimentation pace and upstream flood water levels following a medieval tidal-river diversion catastrophe (biesbosch, the netherlands, 1421–1750ad). Geomorphology 118, 65–79. https://doi.org/10.1016/j.geomorph.2009.12.009.
Kleinhans, M. G., Cohen, K. M., Hoekstra, J., & IJmker, J. M. (2011). Evolution of a bifurcation in a meandering river with adjustable channel widths, Rhine delta apex, The Netherlands. Earth Surf. Process. Landf., 36. doi:https://doi.org/10.1002/esp.2222.
Kleinhans, M.G., Ferguson, R.I., Lane, S.N., Hardy, R.J., 2013. Splitting rivers at their seams: bifurcations and avulsion. Earth Surf. Process. Landf. 38, 47–61. https://doi.org/10.1002/esp.3268.
Macklin, M.G., Toonen, W.H., Woodward, J.C., Williams, M.A., Flaux, C., Marriner, N., Nicoll, K., Verstraeten, G., Spencer, N., Welsby, D., 2015. A new model of river dynamics, hydroclimatic change and human settlement in the nile valley derived from meta-analysis of the holocene fluvial archive. Quat. Sci. Rev. 130, 109–123. https://doi.org/10.1016/j.quascirev.2015.09.024.
Makaske, B., Maas, G.J., van Smeerdijk, D.G., 2008. The age and origin of the Gelderse IJssel. Neth. J. Geosci. 4, 323–337. https://doi.org/10.1017/S0016774600023386.
Millard, C., Hajek, E.A., Edmonds, D.A., 2017. Evaluating controls on crevasse-splay size: implication for floodplain-basin filling. J. Sediment. Res. 87, 722–739. https://doi.org/10.2110/jsr.2017.40.
Morozova, G.S., Smith, N.D., 2000. Holocene avulsion styles and sedimentation patterns of the Saskatchewan River, Cumberland Marshes, Canada. Sediment. Geol. 130, 81–105. https://doi.org/10.1016/S0037-0738(99)00106-2.
Pierik, H.J., van Lanen, R.J., 2019. Roman and early-medieval habitation patterns in a delta landscape: The link between settlement elevation and landscape dynamics. Quat. Int. 501, 379–392. https://doi.org/10.1016/j.quaint.2017.03.010.
Pierik, H.J., Stouthamer, E., Cohen, K.M., 2017. Natural levee evolution in the Rhine-Meuse delta, the Netherlands, during the first millennium CE. Geomorphology 295, 215–234. https://doi.org/10.1016/j.geomorph.2017.07.003.
Sass-Klaassen, U., Hanraets, E., 2006. Woodlands of the past—the excavation of wetland woods at zwolle-stadshagen (the netherlands): growth pattern and population dynamics of oak and ash. Neth. J. Geosci. 85, 61–71.
Shields, A., 1936. Anwendung der Aehnlichkeitsmechanik und der Turbulenzforschung auf die Geschiebe- bewegung. Ph.D. Thesis. Technical University Berlin.
Singh, V.P., Scarlatos, C.A., 1988. Analysis of gradual earth-dam failure. J. Hydraul. Eng. 114, 21–42. https://doi.org/10.1061/(ASCE)0733-9429(1988)114:1(21).
Slingerland, R.L., Smith, N.D., 1998. Necessary condition for a meandering-river avulsion. Geology 26, 435–438. https://doi.org/10.1130/0091-7613(1998)026<0435.
Smith, N.D., Cross, T.A., Dufficy, J.P., Clough, S.R., 1989. Anatomy of an avulsion. Sedimentology 36, 1–23. https://doi.org/10.1111/j.1365-3091.1989.tb00817.x.
Spruyt, A., Asselman, N., 2017. Afvoerverdeling rijntakken: Eenvoudig regelbaar of niet? Technical Report Deltares Project 11200539-000 Delft, the Netherlands
Stouthamer, E., Berendsen, H., 2000. Factors controlling the Holocene avulsion history of the Rhine-Meuse Delta (The Netherlands). J. Sediment. Res. 70, 1051–1064. https://doi.org/10.1306/033000701051.
Stouthamer, E., Berendsen, H.J.A., 2001. Avulsion frequency, avulsion duration, and interavulsion period of Holocene Channel Belts in the Rhine-Meuse Delta, The Netherlands. J. Sediment. Res. 71, 589–598. https://doi.org/10.1306/112100710589.
Toonen, W.H.J., 2013. A Holocene flood record of the Lower Rhine. Ph.D. Thesis Utrecht Studies in Earth Sciences, p. 41.
Toonen, W.H.J., Foulds, S.A., Macklin, M.G., Lewin, J., 2017. Events, episodes, and phases: signal from noise in flood-sediment archives. Geology 45, 331–334. https://doi.org/10.1130/G38540.1.
Toonen, W.H.J., Munoz, S.E., Cohen, K.M., Macklin, M.G., 2020. High-resolution sedimentary paleoflood records in alluvial river environments: a review of recent methodological advances and application to flood hazard assessment. Palaeohydrology, 213–228. https://doi.org/10.1007/978-3-030-23315-0_11.
Törnqvist, T.E., Kidder, T.R., Autin, W.J., van der Borg, K., de Jong, A.F.M., Klerks, C.J.W., Snijders, E.M.A., Storms, J.E.A., van Dam, R.L., Wiemann, M.C., 1996. A revised chronology for mississippi river subdeltas. Science 273, 1693–1696. https://doi.org/10.1126/science.273.5282.1693.
Van der Meulen, B., Cohen, K.M., Pierik, H.J., Zinsmeister, J.J., Middelkoop, H., 2020. LiDAR derived high resolution palaeo DEM construction workflow and application to the early medieval Lower Rhine valley and upper delta. Geomorphology 370. https://doi.org/10.1016/j.geomorph.2020.107370.
Van der Meulen, B., Bomers, A., Cohen, K.M., Middelkoop, H., 2021. Late Holocene flood dynamics and magnitudes in the Lower Rhine river valley and upper delta resolved by two-dimensional hydraulic modelling. Earth Surf. Process. Landf. 46, 853–868. https://doi.org/10.1002/esp.5071.
van Popta, Y.T., Cohen, K.M., Vos, P.C., Spek, T., 2020. Reconstructing medieval eroded landscapes of the north-eastern Zuyder Zee (the Netherlands): a refined palaeogeographical time series of the Noordoostpolder between a.d. 1100 and 1400. Landscape History 41, 27–56. https://doi.org/10.1080/01433768.2020.1835180.
van Rijn, L.C., 1993. Principles of Sediment Transport in Rivers, Estuaries and Coastal Seas. Aqua Publications.
Vermeulen, B., Haveman, E., 2008. Bureauonderzoek, geofysisch en geomorfologie in het plangebied Bolwerksplas, Worp en Ossenwaard. Ruimte voor de Rivier, fasedocument archeologie, Fase 2. Rapportages Archeologie Deventer. Gemeente Deventer.